3D Progressive Damage Modeling for Laminated Composite Based on Crack Band Theory and Continuum Damage Mechanics

John T. Wang
NASA Langley Research Center
Hampton VA
Evan J. Pineda
NASA Glenn Research Center
Cleveland OH
Vipul Ranatunga
Air Force Research Laboratory
Dayton OH
Stanley S. Smeltzer
NASA Langley Research Center
Hampton VA

ABSTRACT

A simple continuum damage mechanics (CDM) based 3D progressive damage analysis (PDA) tool for laminated composites was developed and implemented as a user defined material subroutine to link with a commercially available explicit finite element code. This PDA tool uses linear lamina properties from standard tests, predicts damage initiation with an easy-to-implement Hashin-Rotem failure criteria, and in the damage evolution phase, evaluates the degradation of material properties based on the crack band theory and traction-separation cohesive laws. It follows Matzenmiller et al.'s formulation to incorporate the degrading material properties into the damaged stiffness matrix. Since nonlinear shear and matrix stress-strain relations are not implemented, correction factors are used for slowing the reduction of the damaged shear stiffness terms to reflect the effect of these nonlinearities on the laminate strength predictions. This CDM based PDA tool is implemented as a user defined material (VUMAT) to link with the Abaqus/Explicit code. Strength predictions obtained, using this VUMAT, are correlated with test data for a set of notched specimens under tension and compression loads.

INTRODUCTION

Composites are lightweight and can be tailored to have superior stiffness and strength in loading directions. Thus, they have been widely used in primary aircraft structures. Composites are less damage tolerant than metals which can yield to redistribute loads. In addition, damage modes of composites are complex and can be difficult to detect. The building block approach has been used for development and certification of composite structures [1, 2], however, this approach is time consuming and requires a large quantity of costly tests. To reduce the time and cost for development and certification of new composite aircraft structures, high fidelity progressive damage analysis (PDA) tools that can reliably predict the onset of damage and damage progression in composite structures are needed.

Many PDA tools have been developed and used [3-13]; however, accurately predicting the failure load of a composite structure is still a very challenging problem. A few traditional failure criteria have been widely used for predicting the damage initiation, such as the maximum stress criteria, the Hashin criteria [14], Hashin-Rotem criteria [15] and the Tsai-Wu [16] criteria. More recently developed failure criteria can be found in Refs. 17 to 19. There are various approaches for degrading ply properties in the damage evolution process [20]. For example, the stiffness of a damaged ply can be exponentially degraded, linearly degraded, or instantaneously degraded to zero [5-8]. The instantaneous degradation approach has been found to be too conservative and can predict lower structural strength than that determined by test data. Recent studies [9, 10] show that lamina property degradations after damage initiation can be modeled by using the crack band theory [9, 21]. The damage evolution process can thus be modeled as the opening of a cohesive crack. In the finite element analysis, the crack opening displacement is smeared into the damaged element using the characteristic length of the element resulting in a greater element strain, which in turn reduces the material property of the element. The characteristic length scale used in the crack band theory can also alleviate mesh dependency issues [22] often encountered in PDA. Furthermore, progression of damage in composite laminates often involves 3D stresses, including in-plane and transverse stresses. To include these stresses in the damage progression analysis, 3D PDA tools are required.

In this study, a simple continuum damage mechanics (CDM) based 3D PDA tool is developed and implemented as a user defined material subroutine to link with a commercial finite element analysis software for laminated composite structures. The user defined material subroutine can be used as a framework for future development of more accurate and advanced PDA capabilities. The CDM approach [23-28] is well developed and easier to implement than discrete damage modeling [12, 13, 29, 30] approaches. In the CDM approach, damage is homogenized and treated as degradation of the material properties, thus no discrete cracks are modeled. This CDM based 3D PDA tool uses linear lamina properties from standard tests, predicts damage initiation with an easy-to-implement Hashin-Rotem failure criteria and in the damage evolution phase, evaluates the degradation of material properties based on the crack band theory and traction-separation cohesive laws. It follows Matzenmiller et al.'s formulation [28] to incorporate the degraded material properties into the damaged stiffness matrix. Since nonlinear shear and matrix stress-strain relations [9, 18] are not implemented, correction factors are used for slowing the reduction of the damaged shear stiffnesses to reflect the effect of these nonlinearities on the laminate strength predictions. Furthermore, it implements length scales to alleviate the mesh dependency issue. A user defined material model is developed which links to a commercial explicit finite element analysis code for efficiently solving large linear and nonlinear composite structure problems. The solutions generated by this PDA tool are correlated with the experimental results.

This paper is organized as follows. First, the failure criteria used for determining the damage initiation in a lamina are presented. Second, the use of crack band theory and the traction-separation cohesive laws for determining the material property degradation in the damage evolution process are discussed and the conventional damage indices of all failure modes are defined. Third, a 3D CDM based model is established, using the damage indices as internal state variables. Fourth, the CDM equations for the development of user defined material model (VUMAT) for linking to Abaqus/Explicit [31] software are presented. Next, correlations of predictions with test data are presented. Last, concluding remarks are given at the end of the paper.

FAILURE INITIATION CRITERIA

For a general three-dimensional state of stress in terms of stress acting on the three principal material planes, the strain-based Hashin-Rotem failure criteria [15] used for this study are expressed as,

$$\left(\frac{\varepsilon_{11}}{X_1}\right)^2 = 1 \tag{1}$$

$$\left(\frac{\varepsilon_{22}}{X_2}\right)^2 + \left(\frac{\gamma_{23}}{X_4}\right)^2 + \left(\frac{\gamma_{12}}{X_6}\right)^2 = 1 \tag{2}$$

$$\left(\frac{\varepsilon_{33}}{X_3}\right)^2 + \left(\frac{\gamma_{23}}{X_4}\right)^2 + \left(\frac{\gamma_{13}}{X_5}\right)^2 = 1 \tag{3}$$

where ε_{ii} and γ_{ij} ($i = 1,3$ and $j = 1,3$) are the normal and engineering shear strains and the strain allowables X_i ($i = 1,6$) are defined in Voigt notation as

$$X_i = \frac{Strength_i}{Modulus_i}, \quad i = 1,6 \tag{4}$$

The first failure criterion, Eq. 1, corresponds to the fiber failure, the second failure criterion, Eq. 2, corresponds to in-plane matrix dominated failure, and the third failure criterion, Eq. 3, corresponds to transverse matrix failure.

DAMAGE EVOLUTION AND DEGRADATIONS OF MATERIAL PROPERTIES

Once any of the Eqs. 1 to 3 is satisfied, the corresponding fiber and matrix damage initiates. The subsequent damage growth, namely, damage evolution, follows as the loading increases. The damage modes considered in this study are fiber tension and compression failure, matrix tension and compression failure, and the in-plane and

transverse shear failure. In this study, interlaminar delaminations are not modeled; the effects of delaminations on the strength predictions will be investigated in future studies. The evolution of each damage mode is assumed to follow a corresponding traction-separation law [9]. After damage initiates, it is assumed that the damage localizes and can be modeled as a cohesive crack within the element. As the element loading increases, the opening of the cohesive crack increases further. The crack opening displacement is smeared into the element, using the characteristic length of the element, resulting in increasing the element strain as shown in the Fig. 1. Using the crack band theory [21], the smeared strains of a damaged element are related to the crack opening displacements by [9]

$$l_e \varepsilon_{11} = l_e \varepsilon_{11}^C + \delta_1^f \tag{6}$$

$$l_e \varepsilon_{22} = l_e \varepsilon_{22}^C + \delta_2^m \tag{7}$$

$$l_e^t \varepsilon_{33} = l_e^t \varepsilon_{33}^C + \delta_3^m \tag{8}$$

$$l_e \gamma_{12} = l_e \gamma_{12}^C + 2\delta_{12}^m \tag{9}$$

$$l_e^t \gamma_{13} = l_e^t \gamma_{13}^C + 2\delta_{13}^m \tag{10}$$

$$l_e^t \gamma_{23} = l_e^t \gamma_{23}^C + 2\delta_{23}^m \tag{11}$$

where l_e is a length scale for ply in-plane strains and l_e^t is the length scale for ply transverse strains. Note that ε_{11}^C, ε_{22}^C, ε_{33}^C, γ_{12}^C, γ_{13}^C, and γ_{23}^C are the element damage initiation strains, determined by Eqs. 1 to 3, which remain the same for further load increments. Note that the shear strains γ_{12}^C, γ_{13}^C, and γ_{23}^C are engineering shear strains. In Eqs. 6-11, δ_1^f, δ_2^m, δ_3^m, δ_{12}^m, δ_{13}^m and δ_{23}^m are the crack opening displacements and any incremental change in the element strain after failure initiation is entirely from the crack opening displacement, where δ_1^f, δ_2^m, δ_3^m are normal, opening mode displacements, and δ_{12}^m, δ_{13}^m and δ_{23}^m are shearing mode displacements. Note that in this study, Abaqus 3D reduced integration element, C3D8R [31], is used, thus there is only one integration point for each element. Consequently, l_e is the square root of the element in-plane area, and l_e^t is the element thickness. The use of length scales can mitigate the dependence of the predictions on the mesh size [6, 9, 21, 22].

Pineda and Waas [9] derived the in-plane damaged moduli using the smeared strains and secant cohesive stiffnesses. The detailed derivations of the degraded 2D material properties can be found in Ref. 9. The derivations can be extended to predict degraded 3D lamina properties for a laminate subject to monotonic and proportional loadings. The damaged tensile and shear moduli of a lamina can be expressed as

$$E_{11}=\left\{\frac{1}{E_{110}}+\frac{\varepsilon_{11}-\varepsilon_{11}^{C}}{t_{1C}^{f}\left[1-\frac{l_e t_{1C}^{f}(\varepsilon_{11}-\varepsilon_{11}^{C})}{2G_{FT}}\right]}\right\}^{-1} \tag{12}$$

$$E_{22}=\left\{\frac{1}{E_{220}}+\frac{\varepsilon_{22}-\varepsilon_{22}^{C}}{t_{2C}^{m}\left[1-\frac{l_e t_{2C}^{m}(\varepsilon_{22}-\varepsilon_{22}^{C})}{2G_{MT}}\right]}\right\}^{-1} \tag{13}$$

$$E_{33}=\left\{\frac{1}{E_{330}}+\frac{\varepsilon_{33}-\varepsilon_{33}^{C}}{t_{3C}^{m}\left[1-\frac{l_e^{t} t_{3C}^{m}(\varepsilon_{33}-\varepsilon_{33}^{C})}{2G_{MT}}\right]}\right\}^{-1} \tag{14}$$

$$G_{12}=\left\{\frac{1}{G_{120}}+\frac{\gamma_{12}-\gamma_{12}^{C}}{2t_{12C}^{m}\left[1-\frac{l_e t_{12C}^{m}(\gamma_{12}-\gamma_{12}^{C})}{4G_{IIC}}\right]}\right\}^{-1} \tag{15}$$

$$G_{13}=\left\{\frac{1}{G_{130}}+\frac{\gamma_{13}-\gamma_{13}^{C}}{2t_{13C}^{m}\left[1-\frac{l_e^{t} t_{13C}^{m}(\gamma_{13}-\gamma_{13}^{C})}{4G_{IIC}}\right]}\right\}^{-1} \tag{16}$$

$$G_{23}=\left\{\frac{1}{G_{230}}+\frac{\gamma_{23}-\gamma_{23}^{C}}{2t_{23C}^{m}\left[1-\frac{l_e^{t} t_{23C}^{m}(\gamma_{23}-\gamma_{23}^{C})}{4G_{IIC}}\right]}\right\}^{-1} \tag{17}$$

where E_{110}, E_{220}, E_{330}, E_{120}, E_{130}, and E_{230} are the linear elastic moduli of a unidirectional lamina and E_{11}, E_{22}, E_{33}, G_{12}, G_{13} and G_{23} are the degraded material moduli. G_{FT} and G_{MT} are the fiber and matrix tension fracture toughnesses, respectively, and G_{IIC} is the Mode II critical energy release rate for shear failures. The t_{1C}^{f}, t_{2C}^{m}, t_{3C}^{m}, t_{12C}^{m}, t_{13C}^{m} and t_{23C}^{m} are the maximum tractions of the triangular traction-separation laws [9] and they are assumed to be the stresses corresponding to the initiation strains determined by Eqs. 1 to 3. For material degradations under compression stresses, equations similar to Eqs. 12 to 17 are used. Note that the

unidirectional material properties for IM7/977-3 used in Eqs. 12 to 17 are given in Table I.

Following the conventional definition [26, 28], these damage indices are defined as

$$d_{n1} = 1 - E_{11} / E_{110} \tag{18}$$

$$d_{n2} = 1 - E_{22} / E_{220} \tag{19}$$

$$d_{n3} = 1 - E_{33} / E_{330} \tag{20}$$

$$ds_{12} = 1 - G_{12} / G_{120} \tag{21}$$

$$ds_{13} = 1 - G_{13} / G_{130} \tag{22}$$

$$ds_{23} = 1 - G_{23} / G_{230} \tag{23}$$

Note that at an undamaged state (fully elastic), the index is set to be zero and at a fully damaged state, the index is set to be one. These damage indices are used as internal variables for establishing the 3D continuum damage mechanics model.

3D CONTINUUM DAMAGE MECHANICS (CDM) MODEL

Following the derivations in Ref. 28, the strain and true stress relation can be expressed as

$$\boldsymbol{\varepsilon} = H\boldsymbol{\sigma} \tag{24}$$

The compliance matrix H can be expressed as,

$$H = \begin{bmatrix} \frac{1}{(1-d_1)E_1} & -\frac{\nu_{12}}{E_1} & -\frac{\nu_{13}}{E_1} & 0 & 0 & 0 \\ -\frac{\nu_{21}}{E_2} & \frac{1}{(1-d_2)E_2} & -\frac{\nu_{23}}{E_2} & 0 & 0 & 0 \\ -\frac{\nu_{31}}{E_3} & -\frac{\nu_{32}}{E_3} & \frac{1}{(1-d_3)E_3} & 0 & 0 & 0 \\ 0 & 0 & 0 & \frac{1}{(1-d_4)G_{23}} & 0 & 0 \\ 0 & 0 & 0 & 0 & \frac{1}{(1-d_5)G_{31}} & 0 \\ 0 & 0 & 0 & 0 & 0 & \frac{1}{(1-d_6)G_{12}} \end{bmatrix} \tag{25}$$

Its inverse is the damaged stiffness matrix and the damaged stress-strain relation, i.e. the 3D CDM model, can be expressed as

$$\boldsymbol{\sigma} = C(d)\boldsymbol{\varepsilon} \tag{26}$$

$C(d)$ is the damaged stiffness matrix which can be expressed as

$$C(d) = \begin{bmatrix} C_{11} & C_{12} & C_{13} & 0 & 0 & 0 \\ & C_{22} & C_{23} & 0 & 0 & 0 \\ & & C_{33} & 0 & 0 & 0 \\ & & & C_{44} & 0 & 0 \\ & Symmetry & & & C_{55} & 0 \\ & & & & & C_{66} \end{bmatrix} \tag{27}$$

where

$$C_{11} = (1-d_1)E_1[1-(1-d_2)(1-d_3)\boldsymbol{\nu}_{32}\boldsymbol{\nu}_{23}]/\Delta$$

$$C_{22} = (1-d_2)E_2[1-(1-d_1)(1-d_3)\boldsymbol{\nu}_{13}\boldsymbol{\nu}_{31}]/\Delta$$

$$C_{33} = (1-d_3)E_3[1-(1-d_1)(1-d_2)\boldsymbol{\nu}_{12}\boldsymbol{\nu}_{21}]/\Delta$$

$$C_{12} = (1-d_1)(1-d_2)E_1[(1-d_3)\boldsymbol{\nu}_{31}\boldsymbol{\nu}_{23}+\boldsymbol{\nu}_{21}]/\Delta$$

$$C_{13} = (1-d_1)(1-d_3)E_1[(1-d_2)\boldsymbol{\nu}_{21}\boldsymbol{\nu}_{32}+\boldsymbol{\nu}_{31}]/\Delta$$

$$C_{23} = (1-d_2)(1-d_3)E_2[(1-d_1)\boldsymbol{\nu}_{12}\boldsymbol{\nu}_{31}+\boldsymbol{\nu}_{32}]/\Delta$$

$$C_{44} = (1-d_4)G_{23}$$

$$C_{55} = (1-d_5)G_{31}$$

$$C_{66} = (1-d_6)G_{12}$$

and

$$\Delta = 1-(1-d_2)(1-d_3)\boldsymbol{\nu}_{32}\boldsymbol{\nu}_{23}-(1-d_1)(1-d_3)\boldsymbol{\nu}_{31}\boldsymbol{\nu}_{13}-(1-d_1)(1-d_2)\boldsymbol{\nu}_{21}\boldsymbol{\nu}_{12} - 2(1-d_1)(1-d_2)(1-d_3)\boldsymbol{\nu}_{13}\boldsymbol{\nu}_{21}\boldsymbol{\nu}_{32}$$

Note that d_i ($i = 1,6$) are the damage variables which are functions of damage indices defined by Eqs. 18 to 23. The normal stiffness damaged variables d_1, d_2, and d_3 may be expressed as

$$d_1 = d_{n1} \tag{28}$$

$$d_2 = d_{n2} \tag{29}$$

$$d_3 = d_{n3} \tag{30}$$

Since the fiber damage, matrix damage, and shear damage modes can all affect the shear stiffness reduction, the shear damage variables d_4, d_5, and d_6 may be expressed as the following phenomenological equations

$$d_4 = 1-(1-d_1)(1-\alpha d_2)(1-\alpha d_3)(1-\beta ds_{23}) \tag{31}$$

$$d_5 = 1-(1-d_1)(1-\alpha d_3)(1-\beta ds_{13}) \tag{32}$$

$$d_6 = 1-(1-d_1)(1-\alpha d_2)(1-\beta \mathrm{ds}_{12}) \tag{33}$$

Here, the values of α and β are assumed to be between zero and one. When their values are zero, they do not affect the shear stiffness degradations. When their values are set to one, they have the maximum effect on the shear stiffness degradations. Note that the matrix and shear moduli for a unidirectional ply are assumed to be linear in this study. The α and β may be regarded as correction factors to account for the effect of the nonlinearity of these moduli on the degradation of the damaged shear stiffnesses in Eq. 27. It is expected that nonlinear stress-strain curves for $[90]_n$ and $[45/\text{-}45]_{ns}$ can be used to calibrate the values of α and β. Also, direct implementation of nonlinear stress-strain curves based on the Enhanced Schapery Theory (EST) [9] or the approach used in Ref. 18 may eliminate the need of using the correction factors α and β.

USER DEFINED MATERIAL MODEL (VUMAT) FOR ABAQUS/EXPLICIT

An ABAQUS/Explicit user defined material model (VUMAT) subroutine was developed to implement the CDM based 3D damaged constitutive equations. This VUMAT links to the Abaqus/Explicit code for PDA of laminated composite structures and is suitable for the reduced integration 3D element C3D8R [31]. Implementations for fully integrated 3D elements are possible, but will be more computationally intensive due to more integration points involved. In this VUMAT, the Green-Lagrange strain tensor is used, so it is applicable for material and geometrically nonlinear analyses.

In the conventional CDM approach, the constitutive model is normally expressed in terms of stress-strain relations. When the material exhibits strain-softening behavior, leading to strain localization, this approach results in a strong mesh dependency of the finite element results due to the fact that energy dissipated decreases with mesh refinement [22]. In the crack band theory, the characteristic length scales are used, related to the element size, and the softening part of the constitutive law is expressed as a traction-separation relation. The use of characteristic length scales and traction-separation laws can assure that the energy released during the damage process is per unit area, not per unit volume, this can alleviate the mesh dependency issue [6, 9, 22]. The critical energy release rates (fracture toughnesses) are treated as additional

material parameters for determining the material property degradations in Eqs. 12 to 17. In this VUMAT, the damage indices in Eqs. 18 to 23 are the solution-dependent state variables (SDVs) which each have a value between 0 and 1. A value of 0 means no damage while a value of 1 means total damage. These SDVs can be output for visualization to identify the extent of damage of each failure mode

CORRELATIONS WITH EXPERIMENTAL DATA

The prediction results for notched specimens were correlated with test data. The correlations can be used to verify if the VUMAT is properly coded and to evaluate the accuracy of the predictions.

Experimental Data

Experimental data of open hole tension (OHT) and open hole compression (OHC) specimens [11-13, 32-34] recently tested by the Air Force Research Laboratory (AFRL) were used for the test-analysis correlations. The dimensions of the specimens are shown in Fig. 2. For strain measurement, an extensometer was mounted on the specimen with its knife edges a half inch above and a half inch below the hole center, along the axial direction. These notched specimens were made of IM7/977-3 laminates, containing various lay-up sequences, and were subjected to either tension or compression load [32, 33]. Three different layups were used for both OHT and OHC specimens; $[0/45/90/-45]_{2S}$ and $[60/0/-60]_{3S}$ were used as the strong layups which have 0^o-plies and $[30/60/90/-60/-30]_{2S}$ was used as the weak layup which has no 0^o-plies, to capture different failure modes. The cured average ply thickness was observed to be about 0.127 mm. These specimens were designed, fabricated and tested according to the ASTM standards. The unidirectional ply properties were also obtained using ASTM test standards. The linear elastic properties of a unidirectional IM7/977-3 ply are listed in Table I, which were obtained from Refs. 11-13 and 32-34. The fiber tension fracture toughness G_{FT} and the fiber compression fracture toughness G_{FC} shown in Table I were obtained from Refs. 7 and 35, respectively, for a similar graphite/epoxy system. The matrix tension fracture toughness G_{MT} and the matrix compression fracture toughness G_{MC} shown in Table I were obtained from Refs. 12, 13, and 34 for the IM7/977-3 material system.

Finite Element Model

The finite element model of the OHT and OHC specimens is shown in Fig. 3. Symmetric boundary conditions were used, and thus only the top half of the laminate was modeled. The number of nodes and the number of elements of the largest $[30/60/90/-60/-30]_{2S}$ model are 31,100, and 27,000, respectively. All the analyses were performed using high performance Linux computer clusters. The Abaqus/Explicit analyses were executed in double precision mode and the number of processors specified for each run was 12. The longest wall clock run time was about 20 hours for the $[30/60/90/-60/-30]_{2S}$ OHT model and the shortest run time was about three hours for the $[60/0/-60]_{3S}$ OHC model.

Analysis Results

In order to check the proper implementation of the VUMAT for elastic stiffness prediction of test specimens and to evaluate the sensitivity of the predicted test-specimen strength on the α and β values used, the stress and strain curves of the $[45/0/90/-45]_{2s}$ OHT specimen with different α and β values are plotted in Fig. 4. A comparison with the test data shows that the elastic stiffness is well captured, thus verifying the implementation. In Fig. 4, the predictions using $\alpha = \beta = 0.3$, 0.5 and 0.6 are shown to illustrate that the changes of α and β values can affect the strength predictions. An increase of α and β values causes greater shear stiffness reductions in the damage evolution stage which in turn can lower the predicted strengths. Note that the change of α and β values from 0.3 to 0.6 reduces the predicted strength by only 7%, indicating that the predicted strength is not be not very sensitive to the α and β values used. Similar trends were observed for other layups. For the following tested and predicted strength correlations performed for the OHT and OHC specimens, all the analysis results were obtained with $\alpha = \beta = 0.5$. It was observed that this set of α and β values served as suitable correction factors to slow the shear stiffness reductions for all the cases analyzed and peak loads were reached without encountering any large element distortion problem.

The predicted strengths of the OHT and OHC specimens with three different lay-ups are compared with the experimental data as shown in Table II. The prediction errors with the averaged test data are also presented in the table. These strengths were obtained by dividing the peak load with the total cross-section area. The total cross-section area is the specimen width multiplied by the laminate thickness. For example, the peak load for the quasi-isotropic OHT specimen can be clearly identified from load displacement curve shown in Fig. 5. The predicted strengths and test data are also plotted in Fig. 6 for visual comparisons. The analysis results presented in Table II and Fig. 6 correlate reasonably well with test results, considering the simplicity of this VUMAT implementation. However, some errors are still more than 10%, indicating further development or adoption of advanced PDA tools are needed for more accurate predictions. Since the interlaminar delamination was not modeled in this study, the effect of delamination on the strength prediction needs be investigated in future studies.

To illustrate that all specimens analyzed using $\alpha = \beta = 0.5$ do reach their peak loads, indicated by the accumulation of significant damage across the width of the specimens, the fiber tensile failure for the outermost major load bearing ply (see red arrow) for each OHT specimen is shown in Fig. 7 and the fiber compression failure for the outermost major load bearing ply for each OTC specimen is shown in Fig. 8. These figures indicate that the major load bearing plies are nearly failed after the peak load has been reached. Note that a complete fiber tensile failure is indicated by SDV1 reaching a value of 1.0 in Fig. 7 while a complete fiber compression failure is indicated by SDV2 reaching a value of 1.0 in Fig. 8.

CONCLUDING REMARKS

A simple CDM based 3D PDA tool has been developed and implemented as a user defined material (VUMAT) subroutine to link with a commercial finite element code, ABAQUS/Explicit. This PDA tool uses linear lamina properties from ASTM standard tests, predicts damage initiation with an easy-to-implement Hashin-Rotem failure criteria, and in the damage evolution phase, evaluates the degradation of material properties based on the crack band theory and traction-separation cohesive laws. It follows Matzenmiller et al.'s formulation to incorporate the degrading material properties into the damaged stiffness matrix. The user defined material subroutine can serve as a framework for future development of more accurate and advanced PDA capabilities.

The characteristic length scales related to the crack band theory were used to alleviate the mesh dependency issue often associated with PDA predictions. This VUMAT uses phenomenological parameters to control the shear stiffness degradations. Note that the matrix and shear moduli for a unidirectional ply are assumed to be linear in this study. The α and β may be regarded as correction factors to account for the effect of the nonlinearity of these moduli on the degradation of the damaged shear stiffnesses. In future studies, the α and β values may be judiciously calibrated by using the nonlinear matrix and shear stress-strain curves obtained from simple coupon tests. Preliminary predictions of the strengths were in reasonably good agreement with test data of OHT and OHC specimens with various layups when $\alpha = \beta = 0.5$ was used. However, some errors are still more than 10%, indicating the need for modeling interlaminar delaminations and further development or adoption of advanced PDA tools for more accurate predictions.

REFERENCES

1. Schafrik, R. 2003. "Technology Transition in Aerospace Industry," Briefing presented at the Workshop on Accelerating Technology Transition, National Research Council, Washington DC, November 24, 2003.
2. Furdek, D. 2011. "Aerospace Structural Material Certification," BOE021711-120, http://www.nist.gov/cnst/upload/New-Steel-Presentation-Furdek.pdf
3. Chang, F. K. and K. Y. Chang. 1987. "A Progressive Damage Model for Laminated Composites Containing Stress Concentrations," *J. Compos. Mater.*, 21(9):834-855.
4. Shahid, I. 1993. *Progressive Failure Analysis of Laminated Composites Subjected to In-Plane Tensile and Shear loads*. Ph. D. Dissertation, Stanford University, Palo Alto, CA.
5. Knight, N. F., Jr. 2006. *User-Defined Material Model for Progressive Failure Analysis*, NASA/CR-2006-214526.
6. Lapczyk, I. and J.A. Hurtado. 2007. "Progressive Damage Modeling in Fiber-Reinforced Materials," *Compos. Part A-Appl. S.*, 38(11):2333-2341.
7. Camanho, P. P., P. Maimi and C. G. Davila. 2007. "Prediction of Size Effects in Notched Laminates Using Continuum Damage Mechanics," *Compos. Sci.Techol.*, 67: 2715-2727.
8. Satyanarayana, A. and A. Pzekop. 2010. *Predicting Failure Progression and Failure Loads in Composite Open-Hole Tension Coupons*, NASA/CR-2010-216700.
9. Pineda, E. J. and A. M. Waas. 2013. "Numerical Implementation of a Multiple-ISV Thermodynamically-Based Work Potential Theory for Modeling Progressive Damage and Failure in Fiber-Reinforced Laminates," *Int. J. Fracture*, 182(1):93-122.

10. Pineda, E. J., B. A. Bednarcyk, A. M. Waas and S. M. Arnold. 2013. "Progressive Failure of a Unidirectional Fiber-Reinforced Composite Using the Method of Cells: Discretization Objective Computational Results," *Int. J. Solids Struct.*, 50:1203:1216.
11. Zhang, D., D. K. Patel and A. M. Waas. 2015. "A Novel Two-scale Progressive Failure Analysis Method for Laminated Fiber-Reinforced Composites," AIAA SciTech, 56th AIAA/ASCE/AHS/ASC Structures, Structural Dynamics, and Materials Conference, 5-9 January 2015, Kissimmee, Florida, AIAA 2015-0969.
12. Iarve E. V., K. Hoos, M. Braginsky and E. Zhou. 2015. "Tensile and Compressive Strength Prediction in Laminated Composites by Using Discrete Damage Modeling," AIAA SciTech, 56th AIAA/ASCE/AHS/ASC Structures, Structural Dynamics, and Materials Conference, 5-9 January 2015, Kissimmee, Florida, AIAA 2015-1880.
13. Fang, E., X. Cui and J. Lua. 2015. "A Phantom Paired Element Based Discrete Crack Network (DCN) Toolkit for Residual Strength Prediction of Laminated Composites," AIAA SciTech, 56th AIAA/ASCE/AHS/ASC Structures, Structural Dynamics, and Materials Conference, 5-9 January 2015, Kissimmee, Florida, AIAA 2015-1579.
14. Hashin, Z. 1980. "Failure Criteria for Unidirectional Fiber Composites," *ASME J. Appl. Mech.*, 47(2):329-334.
15. Hashin, Z. and A. Rotem. 1973. "A Fatigue Failure Criterion for Fiber Reinforced Composite Materials," *J. Compos. Mater.*, 7:448–464.
16. Tsai, S. W. and E. M. Wu. 1971. "A General Theory of Strength for Composite Anisotropic Materials," *J. Compos. Mater.*, 5:58-80.
17. Puck A., H. Schurmann, 2002. "Failure Analysis of FRP Laminates by Means of Physically Based Phenomenological Models," *Compos. Sci.Techol.*, 62:1633-1662.
18. Davila C. G., P. P. Camanho and C. A. Rose. 2005. "Failure Criteria for FRP Laminates," *J. Compos. Mater.*, 39(4):323-345.
19. Pinho, S. T., C. G. Davila, P. P. Camanho, L. Iannuci, and P. Robinson. 2005. *Failure Models and Criteria for FRP Under In-Plane or Three-Dimensional Stress States Including Shear Non-Linearity*, NASA/TM-2005-213530.
20. Garnich, M. R. and V. M. K. Akula. 2009. "Review of Degradation Models for Progressive Failure Analysis of Fiber Reinforced Polymer Composites," *ASME Appl. Mech. Rev.*, 62(1):010801-010801-33.
21. Bazant, Z. P. and B. H. Oh. 1983. "Crack Band Theory for Fracture of Concrete," *Mater. Struct.*, 16(93):155-177.
22. Jirasek, M. 2002. "Objective Modeling of Strain Localization," *Revue Francaise Genile Civil*, 6 (6):1119-1132.
23. Kachanov, L. M. 1958. "On the Time of Fracture under Creep Conditions," *Izvestiya Akademii Nauk SSSR, Otdeleniya Tekhnika Nauk*, 8(1):26–31.
24. Kachanov, L. M. 1986. *Introduction to Continuum Damage Mechanics*, Martinus-Nijhoff, Dordrecht.
25. Lemaitre, J. 1996. *A Course on Damage Mechanics*, 2nd ed. Springer, Berlin.
26. Chaboche, J. L. 1988. "Continuum Damage Mechanics: Part II-Damage Growth, Crack Initiation, and Crack Growth," *ASME J. APPL. MECH.*, 55:65-72.
27. Talreja R. 1985. "A Continuum Mechanics Characterization of Damage in Composite Materials," *Proc. R. Soc. Lond.*, A399:195-216.
28. Matzenmiller, A, J. Lubliner and R. L. Taylor. 1995. "A Constitutive Model for Anisotropic Damage in Fiber-Composites," *Mech. Mater.*, 20(2):125–152.
29. A. Belytschko, T., N. Moes, S. Usui, and C. Parimi. 2001. Arbitrary Discontinuities in Finite Elements. *Int. J. Numer. Meth. Eng.*, 50: 993-1013.
30. B. Rudraraju, S. S., A. Salvi, K. Garikipati, and A. M. Waas. 2010. In-Plane Fracture of Laminated Fiber Reinforced Composites with Varying Fracture Resistance: Experimental

Observations and Numerical Crack Propagation Simulations. *Int. J. Solids Struct.*, 47:901-911.

31. Abaqus. 2013. Abaqus Analysis User's Guide (Abaqus Online Documentation), version 6.13. Dassault Systèms Simulia Corp., Providence.
32. Clay, S. and R. Holzwarth. 2014. "Quantitative Assessment of Progressive Damage Tools for Composites," Proceedings of the American Society for Composites 2014-Twenty-nineth Technical Conference on Composite Materials.
33. AFRL Lab Report: Final Report on AIR VEHICLE INTEGRATION AND TECHNOLOGY RESEARCH (AVIATR) Task Order 0037. 2015. *Assessment, Quantification, and Benefits of Applying Damage Tolerant Design Principles to Advanced Composite Aircraft Structure*, AFRL-RQ-WP-TR-2015-0068, February, 2015.
34. Engelstad, S. P. and J. E. Action. 2015. "Assessment of Composite Damage Growth Tools for Aircraft Structure, Part I," AIAA SciTech, 56th AIAA/ASCE/AHS/ASC Structures, Structural Dynamics, and Materials Conference, 5-9 January 2015, Kissimmee, Florida, AIAA 2015-1876.
35. Laffan, M.J., S.T. Pinho, P.R. Robinson, L. Iannuci, A.J. McMillan. 2012. "Measurement of the Fracture Toughness Associated with the Longitudinal Fiber Compressive Failure Mode of Laminated Composites," Composites: Part A, 43:1930-1938.

Table I – MATERIAL PROPERTIES

Material Property	
$E_{110}(GPa)$	164.0 (Tension) 137.4 (Compression)
$E_{220}, E_{330}(GPa)$	8.98
$G_{120}, G_{130}(GPa)$	5.02
$G_{230}(GPa)$	3.00
$\boldsymbol{\nu}_{12}, \boldsymbol{\nu}_{13}$	0.320
$\boldsymbol{\nu}_{23}$	0.496
$G_{IC}, G_{IIC}(N/mm)$	0.256, 1.156
$Y_T, Y_C(MPa)$	100.0, 247.0
$S(MPa)$	80.0
$X_T, X_C(GPa)$	2.90, 1.68
$G_{FT}, G_{FC}(N/mm)$	81.534, 24.533
$G_{MT}, G_{MC}(N/mm)$	0.256, 1.156

Table II – TEST AND ANALYSIS RESULTS

	OHT			OHC		
Lay-Ups	Analysis (MPa)	Test (MPa)	% Error	Analysis (MPa)	Test (MPa)	% Error
$[0/45/90/-45]_{2s}$	508	554	-9.06	318	341	-6.74
$[60/0/-60]_{3s}$	533	543	-1.88	290	358	-18.99
$[30/60/90/-60/-30]_{2s}$	461	409	11.28	327	295	10.85

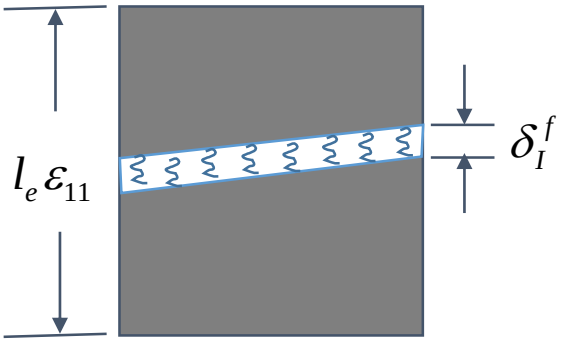

Figure 1. Damaged element with cohesive opening.

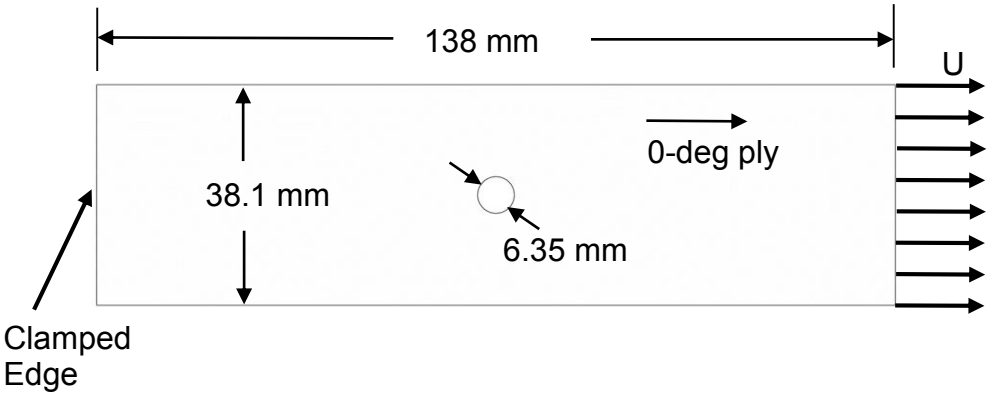

Figure 2. Dimensions of IM7/977-3 open hole specimen.

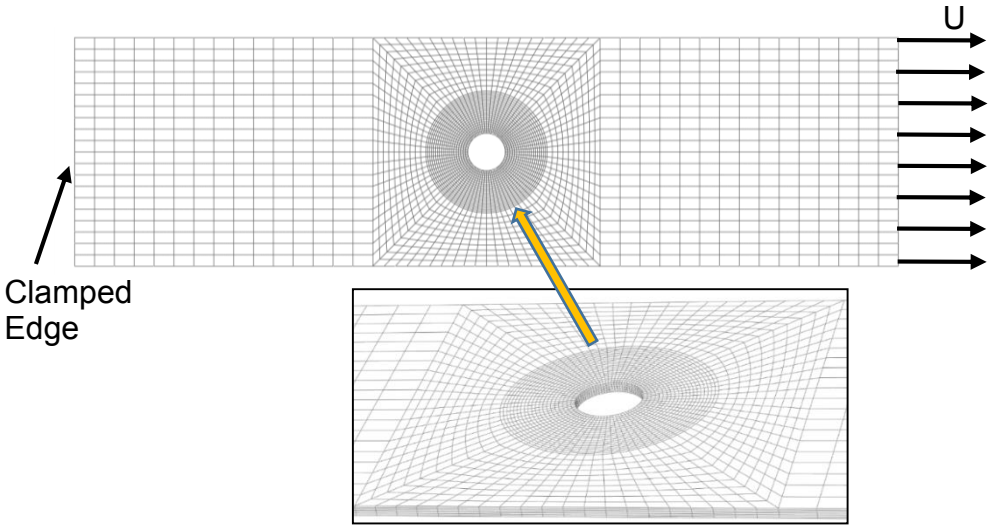

Figure 3. 3D finite element mesh of open hole specimen.

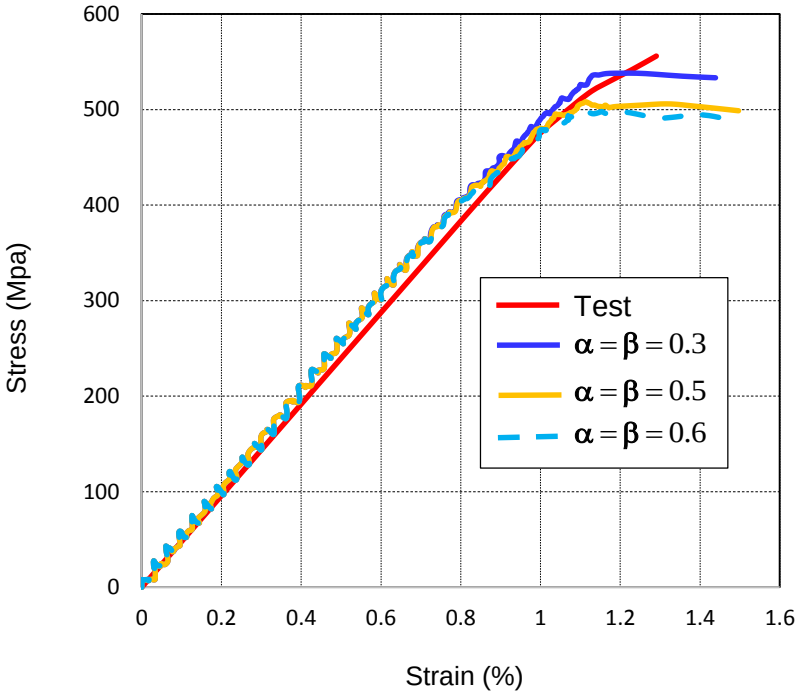

Figure 4. Stress-strain plot for OHT $[0/45/90/-45]_{2S}$ specimen using various values of α and β.

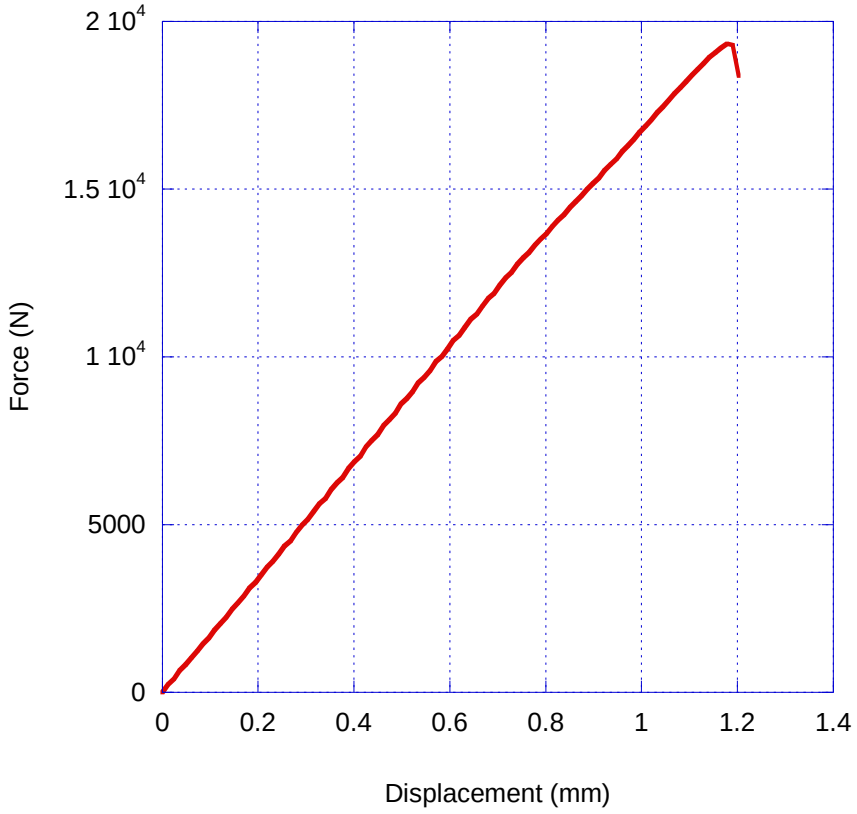

Figure 5. Predicted load-displacement curve for $[0/45/90/-45]_{2S}$ OHT specimen.

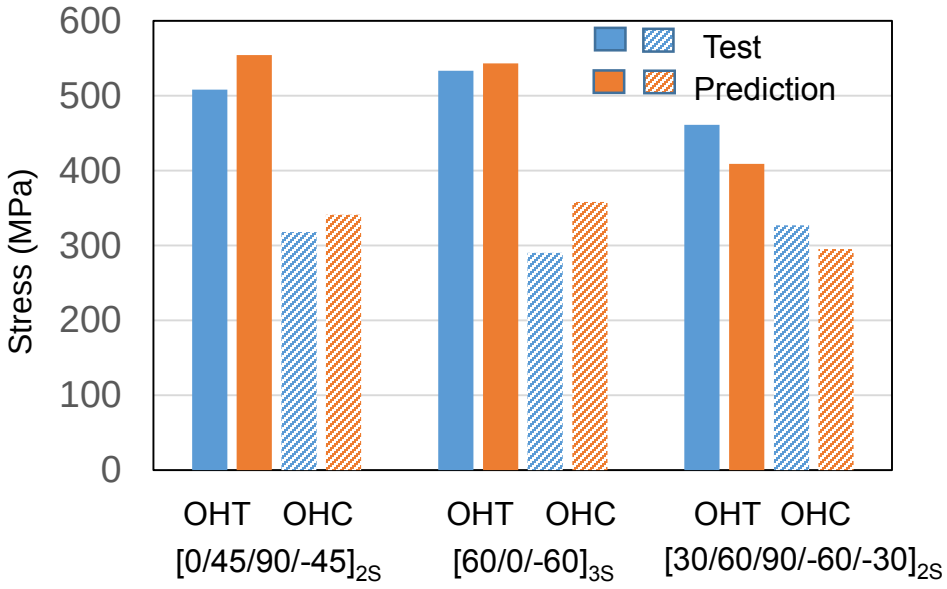

Figure 6. Test and analysis results correlations.

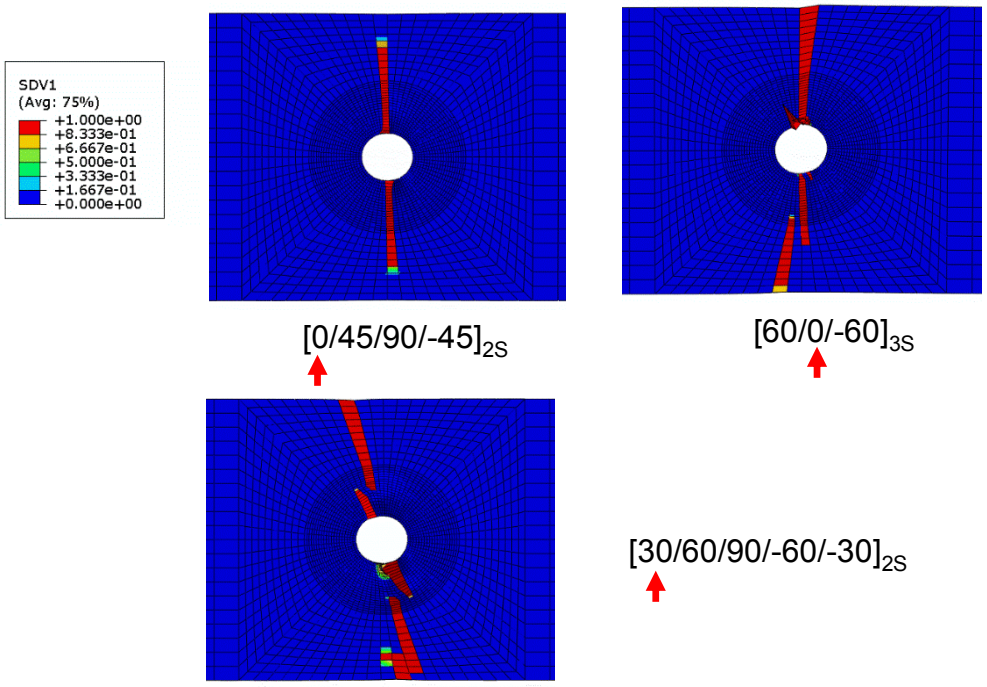

Figure 7. Final fiber tensile failure (SDV1) in outermost major load bearing ply.

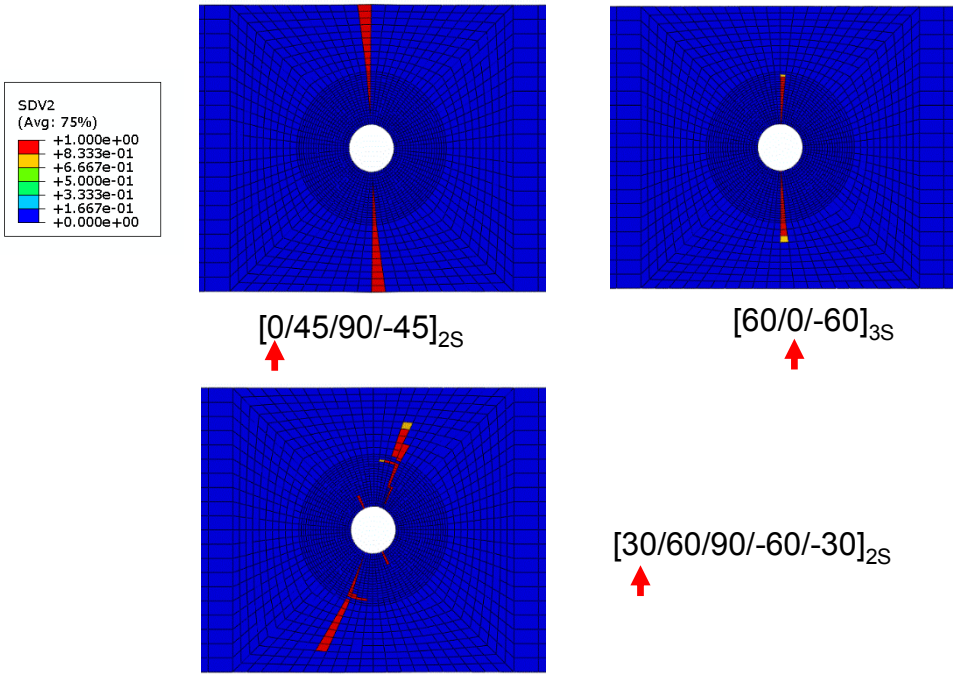

Figure 8. Final fiber compression failure (SDV2) in outermost major load bearing ply.